current issues in molecular biology

MDPI

Article

Investigating Potential 5′ UTR G-Quadruplexes Within NRF2 mRNA

Hatice Esenkaya [1,2,*] and Joe Bryant [3]

[1] School of Life Sciences, Molecular Biology and Genetics, Kilis 7 Aralik University, Kilis 79000, Turkey
[2] Department of Cell and Molecular Biology, Karolinska Institutet, 171 77 Stockholm, Sweden
[3] School of Biosciences, Faculty of Health and Medical Sciences, University of Surrey, Guildford GU2 7XH, UK
* Correspondence: hatice.esenkaya@kilis.edu.tr or hatice.esenkaya@ki.se; Tel.: +90-507-971-5955

Abstract

Post-transcriptional regulation of gene expression is influenced by RNA-binding proteins (RBPs) and small non-coding RNAs that bind to conserved mRNA sequences to modulate mRNA processing. These regulatory molecules affect the structural conformation of mRNAs, creating formations like G-quadruplexes (G4s), which alter translation initiation and regulatory-factor site accessibility. Recent studies have highlighted Nuclear factor erythroid 2–related factor 2 (NRF2) as a key regulator of cellular redox homeostasis and cellular response to oxidative stress. An intriguing feature of NRF2 is the structural formation of its 5′ untranslated region (UTR), which may promote or inhibit translation initiation depending on the cellular context. In this study with minigenes, we provide in vitro evidence of RNA G4s in the NRF2 mRNA's 5′ UTR under basal (no stress) conditions. Achieved via electrophoretic mobility shift assay and fluorescence spectra in the presence of Pyridostatin. Understanding how structural motifs within NRF2 5′ UTRs influence mRNA function provides insights into a common molecular mechanism underlying diseases where NRF2 is dysregulated, like cancers, cardiovascular disease, and neurodegeneration, and highlights potential therapeutic avenues through regulation of NRF2.

Keywords: Nuclear factor erythroid 2–related factor; Pyridostatin; RNA-binding proteins; G-quadruplexes; 5′ untranslated regions; cancer

1. Introduction

The regulation of gene expression is a complex and finely tuned process, with messenger RNA (mRNA) playing a crucial intermediary role between DNA and protein synthesis [1]. The structure of mRNA [2], including its 5′ untranslated region (UTR) [3], 3′ UTR [4], and coding region [5], is pivotal in determining the efficiency and timing of gene expression [6]. While the coding region contains the information for protein synthesis [7], the 5′ and 3′ UTRs serve as key regulatory regions that influence mRNA stability [8], translation initiation [9], and post-transcriptional modifications [10]. The 5′ UTR, located upstream of the coding sequence [11], is particularly important for regulating the initiation of translation [12], and often harbours elements like secondary structures [3], upstream open reading frames (uORFs) [13], and binding sites for regulatory proteins or small RNAs [14]. Meanwhile, the downstream 3′ UTR typically influences mRNA stability [15], intracellular localisation [16], and degradation through elements like microRNA binding sites [17] or polyadenylation signals [18]. Together, these regions contribute to a dynamic regulation of gene expression that allows cells to adapt rapidly to changing conditions [19],

Check for updates

Academic Editor: Chan-Yen Kuo

Received: 15 January 2026
Revised: 29 January 2026
Accepted: 1 February 2026
Published: 2 February 2026

Copyright: © 2026 by the authors. Licensee MDPI, Basel, Switzerland. This article is an open access article distributed under the terms and conditions of the Creative Commons Attribution (CC BY) license.

coordinating the production of proteins essential for cellular function and survival. Understanding the features of UTRs that facilitate post-transcriptional gene regulation will provide valuable insights into their potential implications in diseases where these processes are often dysregulated, such as cancer [20] or neurological disorders [21].

The Nuclear factor erythroid 2–related factor 2 (NRF2) gene plays a crucial role in maintaining cellular homeostasis by regulating several key signalling pathways, including the antioxidant response [22], detoxification processes [23], and cellular defence mechanisms against oxidative stress [24]. Advancements in systems biology and molecular-level multi-omics analysis allow us to investigate the complex interactome between NRF2-related cellular signalling pathways and highlight its potential involvement in diseases from cancers [25] and cardiovascular disease [26] to neurodegeneration [20,27]. This has led to discussions regarding the benefits of NRF2 as a therapeutic target [21,28]. Furthermore, a more complete understanding of the activity and signalling interactome of NRF2 may inform future personalised medicines [29,30]. As a transcription factor, NRF2 activates the expression of various genes involved in protecting cells from damage caused by reactive oxygen species (ROS) [31], heavy metals [32], and other environmental stressors [33]. Under normal 'healthy' conditions, NRF2 is sequestered in the cytoplasm through association with the Kelch-like ECH-associated protein 1 (Keap1) dimer, which facilitates ubiquitination and degradation of NRF2 via the Cullin 3-RING-box protein 1 complex (CUL3-RBX1) [33,34] (Figure 1a, top). However, under oxidative stress, ROS disrupt NRF2-Keap1 interactions, permitting the translocation of NRF2 into the nucleus (Figure 1a, bottom). Here, NRF2 heterodimerises with small Maf (sMaf) proteins and binds to antioxidant response elements (AREs) within promoter regions of its specific gene targets, initiating the transcription of antioxidant and cytoprotective genes to counteract ROS [35,36] (Figure 1a, bottom).

The activity of NRF2 is not only regulated by signalling pathways [37], but also by the structural features of its mRNA [38]. The most canonical structure of RNA molecules are double helices that are formed by Watson–Crick hydrogen-bond patterns between base pairs. Alternative Hoogsteen hydrogen-bond base pairings form in non-Watson–Crick patterns to form increasingly structured helices, such as triplexes and quadruplexes [39]. The 5′ UTR of NRF2 mRNA contains guanine-rich sequences that can form secondary RNA tetra-helical structures called G-quadruplexes (G4s) [40,41] (Figure 1b). The first step in forming a G4 involves a G-quartet. This is formed by four guanine bases interacting via a combination of Hoogsteen and Watson–Crick hydrogen bonds, stabilised by a central monovalent cation (M^+) (Figure 1b, top). The cation that forms the strongest interaction within the G-quartet is potassium (K^+), although other cations may also be centralised, such as ammonium (NH_4^+), sodium (Na^+), and lithium (Li^+), which have increasingly weaker interactions (Figure 1b, top right, green text) [42]. Three stacked G-quartet layers with stable parallel topology, linked to loop regions, form the ultimate RNA G4 structure (Figure 1b). G4-forming G-rich regions, found in many mRNAs, are characterised by loop sequences (Figure 1b, bottom). G4s in other mRNAs have been found to have many effects, including influence on translation through stability adjustment [43], accessibility for ribosome binding [44], and the efficiency of translation initiation [45]. Here, the results indicate the potential presence of such a G4 in the 5′ UTR of NRF2 mRNA, potential methods for investigating its function under different cellular conditions, and possible future therapeutic avenues, which are discussed.

The structural integrity of both the mRNA and the associated regulatory proteins play a pivotal role in NRF2 activation [46]. Changes in the RNA secondary structure [47], or in the interactions between RNA-binding proteins and the mRNA [48], can have profound effects on the ability of NRF2 to respond to stress [49], affecting not only its activation but also its ability to regulate genes that control cellular defence mechanisms [50]. The role

of NRF2 as a master regulator of several interacting cellular signalling pathways places it in a key position to be dynamically regulated by RNA G4s, which have been shown to be modulated under different cellular conditions, such as cellular stress [51]. Such a mechanism would allow for controlled responses to environmental cues. Disruptions in the formation of the structural elements of NRF2 have been shown to contribute to several diseases [20,25]. Thus, a more thorough understanding of how the structural formation of NRF2 mRNAs might influence its regulatory role may open new possibilities for targeted therapeutic interventions.

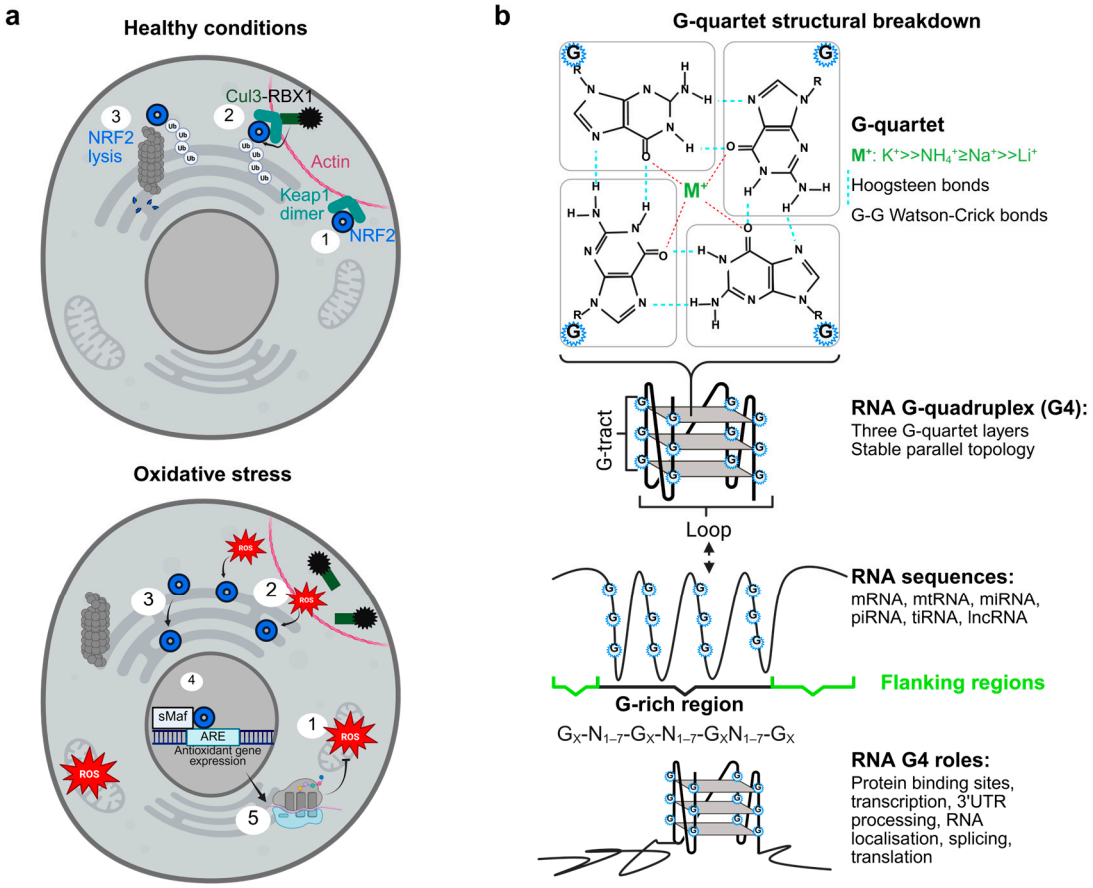

Figure 1. Schematic representation of the NRF2 signalling pathway and the layered structure of RNA G-quadruplexes. (**a**) Under basal 'healthy' conditions (**top**), NRF2 interacts with Kelch-like ECH-associated protein 1 (Keap1) dimers on cytoskeletal actin filaments (1), facilitating ubiquitylation of NRF2 via the Cullin 3-RING-box protein 1 complex (2) in preparation for proteolysis (3). During oxidative stress (**bottom**), ROS disrupt NRF2-Keap1 interactions (1–2), allowing NRF2 translocation into the nucleus (3), whereby NRF2 heterodimerises with small Maf (sMaf) proteins and activates transcription of antioxidant and cytoprotective genes (4), which are translated into proteins that counteract ROS (5). (**b**) Guanine-rich RNA sequences form G-quadruplexes (G4s), firstly by G-quartet formation, relying on a potassium ion K^+ or other ions with decreasing ionic strengths (green text). G-quartets stack to form the RNA G4 and have several important roles in RNA processing.

To investigate the presence of an RNA G4 in the 5′ UTR of NRF2 mRNA, a series of computational and experimental techniques were employed [52]. Initially, a series of bioinformatics tools were used to predict whether these structural motifs exist within the NRF2 RNA sequence [53–56]. To validate in silico predictions, we designed minigenes corresponding to the NRF2 mRNA 5′ UTR to assess the potential for G4 structural formation. We utilised an electrophoretic mobility shift assay (EMSA) [57], with a commonly used G4-specific antibody called 1H6 IgG [58] to investigate RNA G4 formation. The EMSA is a

fundamental technique involving the use of polyacrylamide gel electrophoresis (PAGE) to determine protein–nucleic acid interactions [59]. Protein–nucleic acid complexes are larger than separate molecules and, therefore, diffuse more slowly through the gel; hence, if our minigenes interacted with the 1H6 antibody, they migrated a shorter distance than unbound RNA. Next, we aimed to manipulate this interaction using pyridostatin (PDS) [60,61], a small molecule known to stabilise DNA or RNA G4 structures [62]. The effect of PDS binding to the NRF2 5′ UTR was assessed by fluorescence emission spectroscopy [63]. By quantifying the association of 1–50 μM of PDS with 1 μM of RNA, the dissociation constant (K_d) was calculated [64]. The dissociation suggests how strongly two molecules interact and is given as a concentration (μM) at which half of the complex will separate into individual component molecules. However, this K_d does not always directly relate to in vivo binding efficiency since local concentration, ligand accumulation, and cooperative effects can also enhance in-cell associations. Here, the K_d was measured by plotting the fractions of RNA-complexed vs. individual proteins and performing non-linear regression [65]. The overall goal was to directly measure the formation and stabilisation of RNA G4s in the NRF2 5′ UTR and assess their potential functional relevance.

2. Materials and Methods

2.1. In Vitro Transcription and Purification of NRF2 5′ UTR RNA

Three complementary bioinformatic structural analysis tools—RNAfold (version 2.6.3, default parameters) [66], QGRS Mapper (2006, Min G-run length =2, loop length = 0–36 nucleotides, and min score = 15) [55], and G4Hunter (Threshold = 1.5 and widow size = 20) [56]—were used to assess the human NRF2 gene (Ensembl ID: ENSG00000116044) 5′ UTR (NCBI RefSeq accession number: NM_006164.4) and investigate the presence of an RNA G4 structure. The predicted RNA G4-forming section (spanning nucleotides −197 to −158) was synthesised as two complementary DNA oligonucleotide sequences 5′-GTGGGGCGGGAGGCGGAGCGGGGCAGGGGCCCGCCGGCG-3′and 5′-CACCCCGCCCTCCGCCTCGCCCCGTCCCCGGGCGGCCGC-3′ (Supplementary Figure S1a). The two sequences were annealed in a 1:1 molar ratio to form the DNA template for PCR [67]. This PCR amplification was performed to generate the transcription template (minigene) for in vitro RNA synthesis, and was performed using primers designed to incorporate the T7 RNA-polymerase promoter sequence. This is a common molecular technique adapted from [68]. The forward primer (5′-TAATACGTGGGGCGG-3′) contains the T7 promoter (TAATAC) sequence, and the reverse primer (5′-GCGGCCGCCCGGGGA-3′) is complementary to the end of the NRF2 5′ UTR G-rich region (Supplementary Figure S1b).

The transcription reaction was prepared to a 50 μL final volume including: 40 mM Tris–HCl pH 7.5, 20 mM $MgCl_2$, 10 mM NaCl, 2 mM spermidine HCl, 10 mM DTT, 4 mM rNTPs, 5% RNaseOUT (Invitrogen, Waltham, MA, USA), 10 ng/μL PCR template, 5% T7 polymerase (1: 20 dilutions, homemade). The reaction was held at room temperature for 10 min to allow for proper mixing, followed by incubation for 4 h at 37 °C for transcription. After the transcription reaction, 1 unit of DNase I (Promega, Madison, WI, USA) was added for an additional 30 min at 37 °C to degrade any remaining DNA template. Termination was achieved through a 10 min 65 °C incubation. RNA was purified using an S-300 spin column (GE Healthcare, Chicago, IL, USA), followed by a standard phenol-chloroform extraction to remove residual contaminants. RNA was precipitated at −20 °C for 30 min with 2.5 volumes of ethanol. Centrifugation created an RNA pellet, which was collected, washed with 70% ethanol, and air-dried. The purified RNA was resuspended in RNase-free water and frozen in −80 °C. RNA concentration was assessed using a spectrophotometer by measuring absorbance at 260 nm. RNA fragments were determined to be pure with an A260:A280 ratio of approximately 2.0 according to the Thermo scientific Nanodrop

spectrophotometer (Wilmington, DE, USA) technical bulletin T042. Finally, the integrity of the RNA was confirmed by electrophoresis at room temperature on a 1% agarose gel, ensuring the absence of degradation products (Supplementary Figure S2a).

2.2. End-Labelling of RNA Oligonucleotides

RNA oligonucleotides were 5′ end-labelled using a standard procedure with T4 polynucleotide kinase (PNK) (New England Biolabs, Ipswich, MA, USA) and [γ-32P] ATP (Perkin Elmer, Shelton, CT, USA) [69]. The labelling reaction was set up by combining the following components in a final volume of 20 µL at room temperature: 1× PNK reaction buffer (New England Biolabs, Ipswich, MA, USA), 2.5 µM RNA oligonucleotide template, 0.33 µM [γ-32P] ATP (specific activity: 3000 Ci/mmol, 10 mCi/mL; Perkin Elmer, Shelton, CT, USA), 10 U of T4 polynucleotide kinase (PNK) (New England Biolabs, Ipswich, MA, USA). The reaction was placed at 37 °C for 1 h to allow for phosphorylation of the RNA 5′ end. Following incubation, the labelled RNA was separated by electrophoresis on a 15% denaturing polyacrylamide gel (6 M urea, 1× TBE buffer (89 mM Tris base, 89 mM boric acid, 2 mM EDTA), and 15% acrylamide (19: 1 bisacrylamide) solution (Accugel, Atlanta, GA, USA)) for 3 h at 18 Watts. After electrophoresis, the band corresponding to the labelled RNA was excised from the gel. The RNA was then purified by ethanol precipitation. The gel slice was incubated with 300 mM sodium acetate and centrifuged at 13,000 rpm for 15 min. The resulting pellet was washed with 200 µL of pure ethanol and dried under vacuum for 30 min. After purification, labelled RNA was resuspended in RNase-free water for subsequent experiments.

2.3. Electrophoretic Mobility Shift Assay

EMSA was adapted from experiments described in past papers [57]. Here, DNase I-treated 5′ end-labelled NRF2 5′ UTR mRNA was denatured by incubating at 95 °C for 5 min, then slowly cooled to room temperature overnight. The pure RNA was then incubated with the 1H6 antibody at 0, 1, 5, 10 µM concentrations. The RNA and antibody mixture was incubated at 30 °C for 10 min in a microtitre plate to allow for complex formation. For gel preparation, the RNA–antibody mixture was combined 1: 1 with native bromophenol blue and xylene cyanol gel dyes with 50 mM Tris and 50 mM Glycine. The samples were then added onto a 2.5% (*w*/*v*) native Low Melting Point (LMP) agarose (Invitrogen, Waltham, MA, USA) gel in 1× Tris/Glycine buffer (50 mM Tris, 50 mM Glycine). Electrophoresis was performed at 4 °C at 80 V for 2.5 h in 1× Tris–Glycine buffer. Following electrophoresis, the gels were compressed and dried overnight under vacuum. After drying, the gels were scanned using a Typhoon scanner with a phosphor imaging screen to visualise the labelled RNA. The scanned images were analysed and quantified using OptiQuant software (version 5.0) to determine the size of RNA–antibody complexes and the relative binding efficiency at varying antibody concentrations. This experiment was repeated in two independent biological repeats and quantified in ImageJ (version v1.53c). Analysis and visualisation were done in Microsoft Excel, including normalisation of signals to background and relative calculation of antibody-bound RNA to unbound RNA (Supplementary Data).

2.4. Fluorescence Assays

Fluorescence assays and concentrations of the reagents chosen were adapted from a previously described technique [63]. In our experiment, the mRNA fragment in vitro transcribed in Section 2.1 (5′-GTGGGGCGGGAGGCGGAGCGGGGCAGGGGCCCGCCGGCG-3′) was prepared at a final concentration of 1 µM. This ensured reliable fluorescence detection and binding signal while maintaining physiological relevance and avoiding RNA aggregation. The PDS (MERCK SML2690, Burlington, MA, USA) was added to 1, 2, 5, 10, and 50 µM to span a full titration range for fluorescence binding assays, allowing for the accurate determination of binding affinity. The RNA-PDS mixture was prepared in G4-forming buffer (10 mM KCl,

10 mM Tris–HCl pH 7.5 and 1 mM $MgCl_2$). The solution containing the 1 μM NRF2 mRNA and specific concentrations of PDS was carefully mixed in a Hellma fluorescence cuvette (Suprasil® quartz cuvette, Plainview, NY, USA) with a spectral range of 200–2500 nm and a path length of 10 × 2 mm, chamber volume of 100 μL. The cuvette material and specifications (Suprasil®) were chosen to minimise background fluorescence and allow optimal signal detection for RNA fluorescence assays. The fluorescence emission was recorded at room temperature using FluoroMax-4. The excitation wavelength was set to 555 nm, which is optimal for the excitation of PDS-bound RNA [70]. Emission spectra were collected from 350 nm to 700 nm, as this range encompasses the characteristic emission maxima observed for PDS-bound RNA G4s in two biological replicates (n = 2). Previous studies showed that PDS exhibits enhanced fluorescence upon G4 binding, with emission maxima typically observed around 610–620 nm [70]. The spectra were recorded in 1 nm intervals to ensure accurate resolution of emission features, with the data being collected in scan mode for a full emission profile. We used MATLAB (version R2024B) to create a non-linear regression with the intensities at different PDS concentrations. The fluorescence intensity with no PDS (Fmin) and maximum fluorescence intensity at maximum saturation (Fmax) were used in the binding isotherm equation for K_d calculations (Supplementary Data).

3. Results

To investigate the potential for RNA G4 formation in the 5′ UTR of NRF2 RNA under basal conditions, we employed three bioinformatics tools: RNAfold, QGRS Mapper, and G4Hunter. The sequence of the NRF2 5′ UTR analysed was the same as amplified for in vitro transcription, as described in Section 2.1: 5′-GTGGGGCGGGAGGCGGAGCGGGGCAGGGGCCCGCCGGCG-3′. We compared the predictions from these tools to assess their ability to identify G4-forming regions within this RNA segment (Supplementary Figure S3a–c). RNAfold predicted G4-forming regions based on folding energy and sequence motifs, suggesting that the 5′ UTR sequence 5′-GTGGGGCGGGAGGCGGAGCGGGGCAGGGGCCCGCCGGCG-3′ is likely to harbour a highly stable RNA G4 structure. This tool highlighted the segment 5′-GTGGGGCGGGAGGCGGAGC-3′, which forms an RNA G4 structure of three G-tracts (5G, 3G, and 3G) separated by one-nucleotide loops (C and A), forming a predicted 3-tetrad G4 with short loop lengths, which are typically associated with highly stable G4 structures. RNAfold also predicted a minimum free energy (ΔG) of −6.9 kcal/mol, supporting the idea of a strongly structured RNA G4. Of note, this region includes a highly conserved G-rich motif 5′-GGGGGCGGGAGGG-3′, in agreement with previously identified G4-forming sequences. The predictions from QGRS Mapper and G4Hunter were also consistent in identifying a G4-forming region of the NRF2 5′ UTR 5′-GTGGGGCGGGAGGCGGAGC-3′. All three tools highlighted the same G-rich sequence 5′-GGGGGCGGGAGGG-3′, supporting the likelihood of RNA G4 formation. Together, these results indicate that the formation of G4 structures in this region is likely. To further investigate the potential significance of the proposed RNA G4 complex in the NRF2 5′ UTR, we aligned several representative mammalian NRF2 5′ UTR sequences to explore evolutionary conservation. The G-rich tract highlighted by the three predictive software programmes is partially conserved in a manner that would preserve RNA G4 structural formation (Supplementary Figure S3a–c).

To experimentally verify the RNA G4 formation and assess the binding of the 1H6 antibody to the NRF2 5′ UTR, we conducted EMSA using varying concentrations of the 1H6 antibody (Figure 2). The experiment was run on an LMP gel to assess the binding of the G4 structure without denaturing the RNA. The NRF2 5′ UTR RNA fragment 5′-GTGGGGCGGGAGGCGGAGCGGGGCAGGGGCCCGCCGGCG-3′ was incubated with increasing concentrations of the 1H6 antibody (ranging from 1 to 10 μM) in a binding buffer optimised for RNA G4 stabilisation (Figure 2a, left). As the concentration of

the 1H6 antibody increased, we observed a clear shift in the mobility of the RNA on the native gel. At higher antibody concentrations (1 μM and above), a distinct slow-migrating band appeared, which is consistent with the formation of a stable RNA-1H6 antibody complex. In negative control experiments, we used no antibody, which did not result in any detectable mobility shift, confirming the specificity of the interaction between the 1H6 antibody and the RNA G4 structure (Supplementary Figure S2b). The 1H6 antibody efficiency to an alternative positive control G4 was not included here, but has been shown in previous publications [71]. Furthermore, we used an RNA G4-disrupting mutant where six G residues within the RNA G4 core sequence 5′-GGGGGCGGGAGGG-3′ were substituted with adenines (A) (positions 3–6 and 10–11), resulting in the disrupting mutant sequence: (5′-GTAAAACGGGAGACGGAGCGGGGCAGGGGCCCGCCGGCG-3′). This modified sequence prevents the G-tetrad stacking required for RNA G4 formation. With this mutant, we saw significantly reduced mobility shift of the NRF2 5′ UTR, further confirming that the observed shift was dependent on the presence of a stable G4 structure in the RNA.

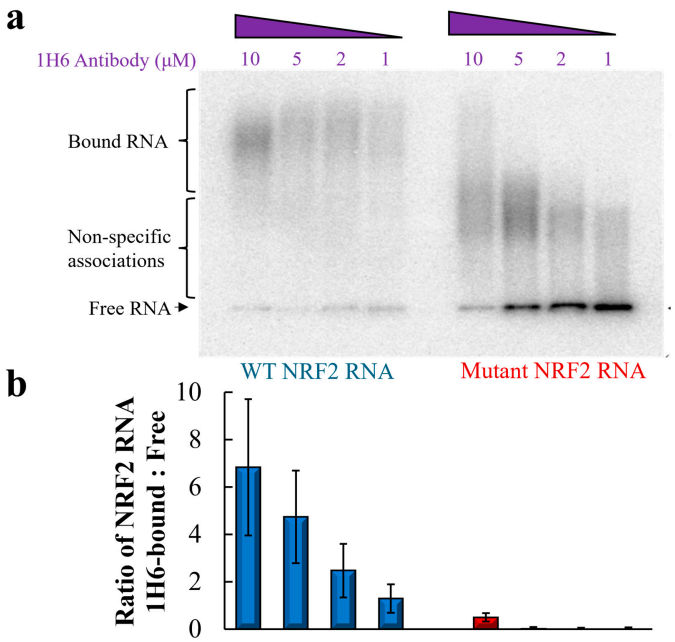

Figure 2. (**a**) Electrophoretic mobility shift assay (EMSA) gel picture of NRF2 RNA G-quadruplex associations with descending concentrations of 1H6 antibody from 10 to 1 μM (purple). Association with wild-type (WT) RNA (blue) as concentration of antibody decreases, binding diminishes, and RNA transitions from bound at the top to non-specific binding or free RNA, moving down through the gel. The G4-disrupting mutant RNA(red) shows RNA G4 binding is prevented across all 1H6 concentrations; only non-specific associations remain. (**b**) EMSA quantification with ImageJ showing the ratio of 1H6 antibody: free NRF2 RNA. Bars refer to the EMSA lanes immediately above them and share the same colour code. Error bars show standard deviation between biological replicates (n = 2).

The 2.5% LMP agarose gel picture shows both WT (left) and mutated NRF2 5′ UTR (right) RNA G4s binding to 1H6 AB in a variety of concentrations (1, 2, 5, and 10 μM). In the WT condition, free RNA shifts upwards due to binding to 1H6 AB as the formation of RNA G4s occur. The mutated form (with base-pair changes from Gs to As) does not show the same upward shift, only some lower non-specific associations, and natural RNA G4s do not form anymore (Figure 2a). The ratio of 1H6 antibody-bound NRF2 RNA: free RNA was calculated from the band intensities of the WT and mutated conditions, normalised to background, or the no-1H6 AB condition (Figure 2b, Supplementary Figure S2b). This semi-quantitative approach suggests that an RNA G4 is forming in this region because associations are visible and proportional to the amount of antibody loaded.

To further characterise the G4 structure formed by the NRF2 5′ UTR RNA, we performed fluorescence spectroscopy, including PDS that selectively binds to RNA G4s, resulting in a change in fluorescence emission due to the interaction with the RNA G4 structure (Figure 3). This assay allowed for the determination of binding affinity based on fluorescence intensity across wavelengths, and provided insight into the formation and stabilisation of a G4 in the 5′ UTR of NRF2 RNA. Following incubation, the fluorescence emission spectra of the DNA-free PDS–RNA complexes were measured between 500 and 600 nm, which represents the emission range of Pyridostatin when bound to RNA G4 structures (Figure 3). A sharp increase in fluorescence intensity at approximately 555 nm was expected as PDS binds to the RNA G4 structure, and any shift or change in intensity would indicate stabilisation of the RNA G4 conformation by PDS (Figure 3a). A control sample containing only RNA and no PDS was included to measure the baseline fluorescence. The fluorescence spectroscopy binding assay confirmed the creation of a stable G4 structure in the 5′UTR of NRF2 RNA and demonstrated that PDS binds specifically to the RNA G4 structure. The fluorescence emission spectra showed a clear, concentration-dependent increase in intensity upon PDS binding. The K_d for binding of PDS to NRF2 RNA was calculated by non-linear regression using Python (version 3.13.1) and MATLAB (version R2024B) tools (Supplementary Data). The K_d value of 29.82 µM indicates a moderate interaction between PDS and the NRF2 RNA G4 (Figure 3b), which agrees with previous RNA G4 measurements ([72,73]).

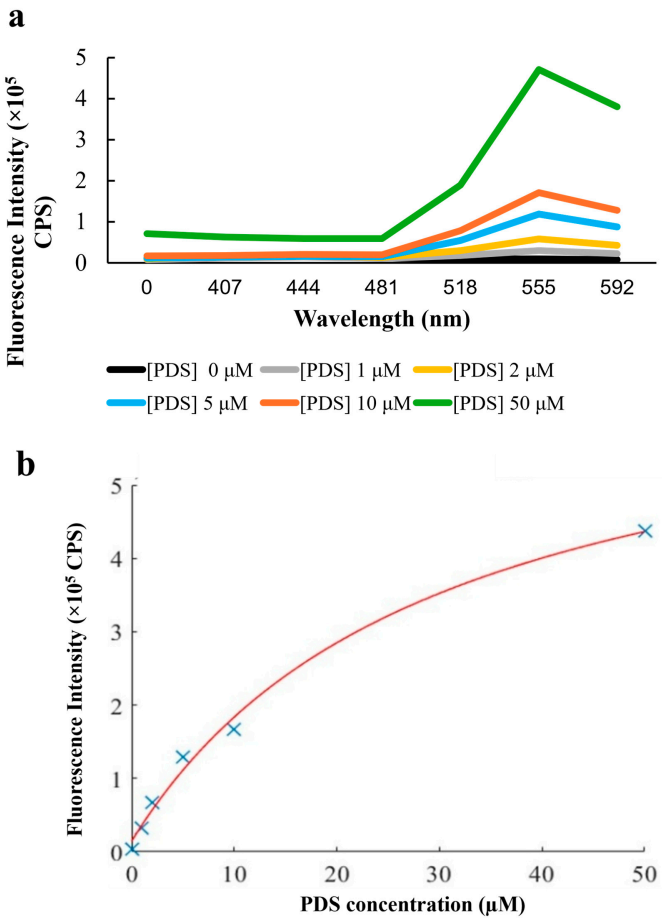

Figure 3. (**a**) Line graph showing the interaction of 0–50 µM of Pyridostatin (PDS) with the NRF2 RNA 5′ UTR G4-forming sequence. Note: 0 µM is black, 1 µM is grey, 2 µM is yellow, 5 µM is blue, 10 µM is orange, and 50 µM is green (n = 2). (**b**) Binding curve showing the association of Pyridostatin (PDS) with NRF2 RNA measured by fluorescence spectroscopy. Data points (blue, ×) represent experimental measurements, and the solid line (red) shows the non-linear regression fit used to determine the dissociation constant (K_d).

Fluorescence emission spectra were measured where 1 μM of NRF2 RNA was incubated with PDS at 0 μM (black), 1 μM (grey), 2 μM (yellow), 5 μM (light blue), 10 μM (orange), and 50 μM (green) and measured with an excitation wavelength of 380 nm. This further suggests an RNA G4 complex may form in the NRF2 5′ UTR, even under basal conditions.

4. Discussion

4.1. NRF2 5′UTR RNA G-Quadruplex Formation

This study aimed to elucidate a potential formation of G4 structures in the NRF2 RNA 5′ UTR and discuss implications in the possible regulation of NRF2 expression. Using three bioinformatics tools—RNAfold, QGRS Mapper, and G4Hunter—we consistently identified an RNA G4-forming region within the NRF2 5′ UTR. All three tools highlighted the G-rich sequence 5′-GGGGGCGGGAGGG-3 as a candidate for RNA G4 formation (Supplementary Figure S3a–c). The high consistency across the predictive tools reinforces the reliability of these findings, particularly the prediction by RNAfold, which showed that this G4 structure is highly stable, with a folding energy of −6.9 kcal/mol. Interestingly, sequence alignment showed there may be some evolutionary conservation of this NRF2 5′ UTR sequence, despite 5′ UTR sequences being typically less conserved across species than coding regions, hinting at some biological importance (Supplementary Figure S1). EMSA experiments were conducted that visually and semi-quantitatively supported the in silico analysis through 1H6 antibody concentration-dependent shifting and, importantly, showed that a G4 mutant could abolish G4 association, implying this 5′-GGGGGCGGGAGGG-3 is a critical sequence for antibody interaction and, thus, RNA G4 formation. While the 1H6 antibody is widely used for RNA G4 detection, the shift during antibody binding does not conclusively establish canonical G4 topology [58].

Henceforth, the predictions and EMSAs were further strengthened with fluorescence spectroscopy to characterise the RNA G4 structure by its association with a G4 binding molecule called PDS [62]. Again, the concentration-dependent increase in fluorescence intensity supported the predicted presence of a G4 structure within this section of the NRF2 5′ UTR and enabled mathematical prediction of a K_d at 29.82 μM. Of note, PDS has been shown to bind to G-rich DNA strands of TERRA and Telomere repeat DNA (TeloDNA), known to form DNA G4 structures with K_d's of 0.66 μM and 0.05 μM, respectively [74]. PDS was also identified as a non-sequence-selective ligand for G4s, which associated with the NRAS DNA G4 with a K_d of 4.1 ± 0.1 μM [75], and bound Zika virus RNA G4s in vitro with a K_d of 4.2 ± 0.4 μM. These values show how PDS can certainly bind G4s, but also that its affinity for DNA G4s is typically higher than for RNA G4s. Hence, this paper's methodology ensured thorough DNase treatment of RNA prior to in vitro assays to ensure this did not affect binding. Future investigations for in vivo analysis may consider alternative RNA-G4 ligands so as to prevent these off-target associations, which represent a major concern due to the high prevalence of G4 motifs in DNA, throughout the transcriptome (total mRNAs), and the translatome (mRNAs being actively translated by ribosomes). Antibodies already exist that can preferentially target RNA G4s over DNA G-quadruplexes [76], but for more specific targeting, structure-based drug design and rigorous selectivity screening will be essential to minimise these risks [77].

Despite some potential drawbacks in future applications, the 29.82 μM calculation from our PDS method is a realistic value with a strong-to-moderate binding affinity to the predicted NRF2 RNA G4. To put this in perspective, other RNA G4s have been discovered with similar micromolar affinities [62], which indicates that, depending on cellular context, this interaction should be physiologically viable in vivo. To extend the comparisons for additional perspectives, there are several RNA G4-targeting molecules in initial drug

screens. A molecule termed 'F1' was found to bind to an RNA G4 in human DHX15 5′ UTR with a K_d of 12.6 μM [73], and 'oxymatrine' associated with a G4 in human vascular endothelial growth factor (hVEGF) mRNA with a K_d of 37.5 μM [72]. These K_d values suggest that the NRF2 RNA G4-PDS associations should be strong enough to consider for future initial in vivo analysis, especially as there is plenty of opportunity to optimise a potential therapeutic ligand for specific associations. However, we acknowledge that further experimental validation, such as RNA G4-specific RNA probes or structural assays, could be applied to confirm these predictions and elucidate their functional significance in vivo.

4.2. Structural Analysis

To confirm the exact structure of our proposed RNA G4, including parallel/antiparallel orientation and tetrad number [78], Nuclear Magnetic Resonance (NMR) or X-ray crystallography may be employed [79,80]. This will be especially important for predictions of potential ligands for testing in vivo RNA-G4 formation. X-ray crystallography requires careful trial-and-error adjustment of several aspects of the buffer—including pH, temperature, ion concentration, and precipitant size/concentration—to optimise crystal formation [81]; however, imaging is much more straightforward once the crystallised structure has been formed. In the case of large protein–RNA complexes, crystallisation may be impossible. NMR can measure structures, and is determined by the spinning of protons in hydrogen atom nuclei, and while it is more difficult to perfect than X-ray crystallography, it can be more useful for imaging dynamics over time with chemical shift mapping [82]. NMR can also struggle to determine large complexes, although isotope and segmental labelling techniques have been applied in the past to investigate complicated structures such as ribonucleoprotein complexes [83]. In the case of visualising large, complicated structures, cryo-electron microscopy (Cryo-EM) could be employed, which involves electron microscopy performed at cryogenic temperatures to detect the electron density and generate a map of the protein–RNA structure. However, the resolution of the image generated is lower than that in X-ray crystallography, so the fine points of the RNA G4 structure may remain elusive. Single-molecule tools like Forster Resonance Energy Transfer (smFRET) have previously been applied to investigate G4s [84–86]. Similar to NMR, smFRET can visualise dynamics and interactions between short RNA sequences (~50–100 nucleotides), labelled RNA, and proteins [87]. However, the fluorophore labels can affect RNA folding and function, so the location of fluorophores on the DNA construct needs to be tightly controlled, and the ionic conditions of the experiment need to be highly regulated to allow for the simultaneous G4 formation and fluorescence imaging. Despite these difficulties, the kinetic and mechanistic data from FRET can synergise well with static structural data from X-ray crystallography or Cyro-EM. Finally, it should be stressed that alternative structures, such as hairpins, may coexist with the G4 in the NRF2 5′ UTR; therefore, SHAPE-MaP could be employed as it is the gold-standard method to probe structural heterogeneity in cells. Overall, each high-resolution imaging method has pros and cons, and it would be best to apply these techniques in tandem to enable more detailed structural analyses of NRF2 G4 complex formation [88].

4.3. Towards Validation of NRF2 RNA G-Quadruplex Activity In Vivo

Importantly, other RNA G4s can influence post-transcriptional gene expression, including mRNA splicing, mRNA transport, ncRNA biogenesis, ncRNA function [89,90], and translation [91–94]. Some of these RNA G4-linked mechanisms have been associated with disease; for example, an RNA G4 within the 5′UTR of cyclin D3 mRNA has been shown to help regulate the cell cycle and the disruption of which has been implicated

in cancers [95]. Therefore, it is possible other G4s, like the one we identified, could also have important biological functions. Since RNA G4s have already been linked to oxidative stress [45,96] and previous research has suggested NRF2 may form an RNA G4 during oxidative stress [44], we hypothesise the G4 in 5′UTR may have an impact along this line. Here, the G4 is also shown under basal conditions in vitro, which may provide more indications on how modulation of NRF2 5′ UTR G4 stability may play a role in fine-tuning NRF2 translation to influence the timing and magnitude of cellular antioxidant responses. There are several possibilities for exactly how this occurs. Under basal conditions, stable RNA G4 structures may act as translational repressors, limiting NRF2 protein synthesis to maintain homeostasis and prevent unwarranted activation of the antioxidant pathway [97,98]. Upon oxidative or electrophilic stress, dynamic remodelling or destabilisation of these RNA G4 motifs, potentially mediated by helicases or RNA-binding proteins, could rapidly relieve translational repression, facilitating a timely increase in NRF2 levels. In this case, pharmacological stabilisation of the RNA G4 with ligands like PDS may prolong the repressive state, attenuating NRF2 translation and downstream antioxidant gene expression to reduce NRF2 overactivity in diseases, such as certain cancers, where NRF2 confers chemoresistance [20]. Conversely, G4 formation in the 5′UTR of NRF2 RNA may increase translation most commonly by stimulating cap-dependent translation initiation by recruitment of the 40S small ribosomal subunit via eukaryotic initiation factors (eIFs) [99,100]. This is common for RNA G4s [3], and has been suggested in a previous paper where the removal of the 5′ UTR resulted in an unresponsive NRF2 mRNA which was not induced by H2O2 during oxidative stress [44]. They found that loss of a 5′ UTR G4 complex prevented elongation factor 1 alpha (EF1a) from associating with the NRF2 mRNA transcript, thereby reducing translation. Therefore, if NRF2 expression is no longer enhanced upon oxidative stress, then it cannot upregulate the expression of antioxidant genes as per its normal function. Dysregulation of NRF2 in such a way is linked to various diseases, including cardiovascular [26], Huntington's [27], cancers, and more generally across neurodegeneration [20]. Hence, it has potential as a therapeutic target in the future.

Although current results suggest a possible regulatory role, direct evidence linking the RNA G4 structure to NRF2 expression regulation or cellular responses is lacking, especially relating to the timing or magnitude of NRF2 activation in response to stress. Investigating how RNA G4 stability influences the kinetics of NRF2 activation, including the onset, peak, and duration of protein expression following stress, is therefore crucial. Time-course experiments measuring NRF2 protein and target gene induction, coupled with real-time monitoring of the RNA G4 folding status (e.g., via live-cell RNA imaging, chemical shift mapping NMR spectroscopy, or Forster Resonance Energy Transfer), would provide valuable mechanistic insights into this potential regulatory layer [82,86]. Other functional studies, such as luciferase reporter assays, RNA-binding protein knockdowns/overexpression, or CRISPR-CAS9 experiments, are required to establish if NRF2 expression is changing upon RNA G4 binding in vivo. Luciferase reporter assays have been applied in this manner before to investigate c-MYC transactivation in NM23-H2 binding to a DNA G4 motif within the cMYC gene [101]. For NRF2, reporter constructs containing the wild-type versus RNA G4-disrupting mutant NRF2 5′ UTR sequences could be transfected into cells to quantitatively assess the impact of G4 formation on translational efficiency and RNA stability in living cells. Luciferase reporter assays are useful as they are quick and provide precise quantitative results, although they have limitations too. The main limitation is that the levels of mRNA produced from the plasmid are difficult to match endogenous levels, so they do not completely reflect in vivo conditions, which may be an issue if binding efficiency depends on concentration [102]. Alternatively, CRISPR-Cas9 could be used to create an endogenous NRF2 mutant that can no longer form the RNA

G4 and investigate the effect on the cell's response to oxidative stress with phenotypic cell-culturing experiments [103]. The disadvantage here is that strain generation takes longer, but apart from the mutation, endogenous transcription and translation are maintained, meaning that optimal investigation of the cellular effect of RNA G4 removal is possible. Finally, CRISPR or siRNA interference techniques could be used to knock down RNA-binding proteins known to interact with RNA G4s, such as helicases [104], to evaluate their roles in modulating NRF2 RNA G4 structure stability, consequent NRF2 expression changes, and oxidative stress response. This will be more useful once a clear target to investigate is discovered, so cause-and-effect of NRF2 RNA G4 and the knockdown protein can be clarified.

RNA G4 dynamics are often influenced by cellular context and interacting proteins. Cellular factors that could influence G4 formation and stability include RNA-binding proteins (RBPs), secondary RNA structures, and intracellular ionic conditions. It is well known that RNA G4 complexes are targets for RBPs, which are often required for the physiological effect of the RNA G4 [94]. In vivo, it has also been suggested that cytosine methylation may influence RNA G-quadruplex formation. It is possible that other RNA modifications, such as m7G methylation, also affect RNA G4 structures, possibly acting as rapid switches to activate or inactivate the G4 folding [105]. This is one potential mechanism for how NRF2's RNA G4 may contribute to the oxidative stress response. If the G-rich element is methylated, it may trigger the formation of the RNA G4 and initiate its transcription factor activity. Finally, in vitro, G4 structures are induced by cationic concentrations, most often K^+ [106], so it is possible that the influx of K^+ in vivo may also act as an initiator of RNA G4 folding and be used to initiate the translation of NRF2 to boost antioxidant gene transcription upon oxidative stress. Each of these effects would be missed or exaggerated in our bioinformatics and in vitro experiments, highlighting the need for comprehensive in vivo experiments as the next stage of testing NRF2 RNA G4 cellular function to evaluate pharmacodynamics, toxicity, and long-term effects. There are options for in vivo profiling of the NRF2 RNA G4 with specific probes. For example, fluorescent ligands, like PDS, BRACO-19, TMPyP4, and Ber, can be applied to cells [45,107,108]. These cells can be tested for fluorescence with flow cytometry and immunofluorescence assays to investigate interactions. However, their analysis is limited by the same factors as the NRF2 RNA G4 therapeutic molecule design, by difficulties targeting probes to a subcellular location and a specific RNA-G4 of interest. There is also some difficulty visualising fluorescence in certain subcellular localisations, so new methods and ligands are being explored, such as the RNA G4-ligand guided immunofluorescence staining approach with BrdU-immune-tag–modified G4-ligands for in vivo applications [85]. For initial experiments, PDS could be used as a starting point for NRF2 RNA G4s, as we have shown a relatively strong interaction in vitro.

4.4. Future Perspectives on RNA Therapeutics

Once the prior challenges have been overcome, there is a possibility for therapeutic drug screening methods to find compounds that associate with sufficient efficiency and selectivity. This can be completed in silico via computational docking, which predicts ligands for structure-based drug discovery [109]. However, inconsistencies have been shown within the results from various docking software programmes, such as AutoDock Vina (v1.2.0), DOCK6 (v6.9), Glide, and RxDock (v21.1.0.20298) (each accessed in 2020), when investigated in a paper looking to design a drug targeting a DNA G4 in the MYC promoter [110]. Therefore, biochemical and biophysical high-throughput screening techniques can be employed in tandem with in silico approaches [73]. For example, small-molecule microarrays have been employed recently alongside in silico analysis to discover BMVC, a drug that can target the aforementioned DNA G4 in the MYC promoter [79]. Indeed, there

are many RNA G4s already being exploited by the design of small molecules or aptamers that can bind to the G4 and affect translation for therapeutic purposes [72]. For example, targeted degradation complexes have been developed to specifically degrade RNAs with G4s to inhibit Fragile X mental retardation protein (FMRP), whose overexpression has been associated with metastasis and immune evasion in cancers [111]. Outside genetic defects, DNA G4s have also been targeted for antiviral therapies [112]. For example, the d(GGGT)4) or T30175 aptamers form DNA G4 dimers recognised by the Human Immunodeficiency Virus (HIV) integrase protein, which then competes with viral DNA G4s. Viral DNA G4s are important for replication, and by preventing HIV integrase binding, infectivity is inhibited [113,114]. This shows that although some major developments are required for G4 therapeutics, they are possible and could be applied to NRF2.

5. Conclusions

Together, our novel combination of bioinformatic and in vitro analysis has identified and validated an RNA G4 in the 5′ UTR of NRF2 during in vitro conditions and set up future experiments in vivo using G4-specific probes to provide further insights into the relevance of this structure in cellular contexts. Additionally, structural studies employing high-resolution techniques could be applied to confirm the RNA G4 topology and identify potential interactions with RNA-binding proteins or small molecules. These steps may be used to reveal if NRF2 RNA G4 is a therapeutic target for drug screening and disease treatments.

Supplementary Materials: The following supporting information can be downloaded at https://www.mdpi.com/article/10.3390/cimb48020171/s1.

Author Contributions: Conceptualisation, H.E.; methodology, H.E.; software, H.E. and J.B.; validation, H.E.; formal analysis, H.E. and J.B.; investigation, H.E. and J.B.; resources, H.E.; data curation, H.E. and J.B.; writing—original draft preparation, H.E.; writing—review and editing, H.E. and J.B.; visualisation, H.E.; project administration, H.E. All authors have read and agreed to the published version of the manuscript.

Funding: This research received no external funding.

Institutional Review Board Statement: Not applicable.

Informed Consent Statement: Not applicable.

Data Availability Statement: The original contributions presented in this study are included in the article/Supplementary Materials. Further inquiries can be directed to the corresponding author.

Conflicts of Interest: The authors declare no conflicts of interest.

References

1. Boo, S.H.; Kim, Y.K. The Emerging Role of RNA Modifications in the Regulation of MRNA Stability. *Exp. Mol. Med.* **2020**, *52*, 400–408. [CrossRef]
2. Leppek, K.; Byeon, G.W.; Kladwang, W.; Wayment-Steele, H.K.; Kerr, C.H.; Xu, A.F.; Kim, D.S.; Topkar, V.V.; Choe, C.; Rothschild, D.; et al. Combinatorial Optimization of MRNA Structure, Stability, and Translation for RNA-Based Therapeutics. *Nat. Commun.* **2022**, *13*, 1536. [CrossRef]
3. Leppek, K.; Das, R.; Barna, M. Functional 5′ UTR MRNA Structures in Eukaryotic Translation Regulation and How to Find Them. *Nat. Rev. Mol. Cell Biol.* **2018**, *19*, 158–174, Correction in *Nat. Rev. Mol. Cell Biol.* **2018**, *19*, 673. [CrossRef]
4. Chang, J.W.; Zhang, W.; Yeh, H.S.; De Jong, E.P.; Jun, S.; Kim, K.H.; Bae, S.S.; Beckman, K.; Hwang, T.H.; Kim, K.S.; et al. MRNA 3′-UTR Shortening Is a Molecular Signature of MTORC1 Activation. *Nat. Commun.* **2015**, *6*, 7218. [CrossRef] [PubMed]
5. Narula, A.; Ellis, J.; Taliaferro, J.M.; Rissland, O.S. Coding Regions Affect MRNA Stability in Human Cells. *RNA* **2019**, *25*, 1751–1764. [CrossRef] [PubMed]
6. Buxbaum, A.R.; Haimovich, G.; Singer, R.H. In the Right Place at the Right Time: Visualizing and Understanding MRNA Localization. *Nat. Rev. Mol. Cell Biol.* **2015**, *16*, 95–109, Erratum in *Nat. Rev. Mol. Cell Biol.* **2015**, *16*, 513. [CrossRef] [PubMed]

7. Noller, H.F. Evolution of Protein Synthesis from an RNAworld. *Cold Spring Harb. Perspect. Biol.* **2012**, *4*, a003681. [CrossRef]
8. Cetnar, D.P.; Hossain, A.; Vezeau, G.E.; Salis, H.M. Predicting Synthetic MRNA Stability Using Massively Parallel Kinetic Measurements, Biophysical Modeling, and Machine Learning. *Nat. Commun.* **2024**, *15*, 9601. [CrossRef] [PubMed]
9. Jia, L.; Mao, Y.; Ji, Q.; Dersh, D.; Yewdell, J.W.; Qian, S.-B. Decoding MRNA Translatability and Stability from 5′ UTR. *Nat. Struct. Mol. Biol.* **2020**, *27*, 814–821. [CrossRef]
10. Wei, W.; Gao, W.; Li, Q.; Liu, Y.; Chen, H.; Cui, Y.; Sun, Z.; Liu, Z. Comprehensive Characterization of Posttranscriptional Impairment-Related 3′-UTR Mutations in 2413 Whole Genomes of Cancer Patients. *npj Genom. Med.* **2022**, *7*, 34. [CrossRef]
11. Chu, Y.; Yu, D.; Li, Y.; Huang, K.; Shen, Y.; Cong, L.; Zhang, J.; Wang, M. A 5′ UTR Language Model for Decoding Untranslated Regions of MRNA and Function Predictions. *Nat. Mach. Intell.* **2024**, *6*, 449–460, Correction in *Nat. Mach. Intell.* **2024**, *6*, 988. [CrossRef]
12. van der Velden, A.W.; Thomas, A.A. The Role of the 5′ Untranslated Region of an MRNA in Translation Regulation during Development. *Int. J. Biochem. Cell Biol.* **1999**, *31*, 87–106. [CrossRef]
13. Ryczek, N.; Łyś, A.; Makałowska, I. The Functional Meaning of 5′UTR in Protein-Coding Genes. *Int. J. Mol. Sci.* **2023**, *24*, 2976. [CrossRef] [PubMed]
14. Van Nostrand, E.L.; Freese, P.; Pratt, G.A.; Wang, X.; Wei, X.; Xiao, R.; Blue, S.M.; Chen, J.Y.; Cody, N.A.L.; Dominguez, D.; et al. A Large-Scale Binding and Functional Map of Human RNA-Binding Proteins. *Nature* **2020**, *583*, 711–719, Correction in *Nature* **2021**, *589*, E5. [CrossRef] [PubMed]
15. Szostak, E.; Gebauer, F. Translational Control by 3′-UTR-Binding Proteins. *Brief. Funct. Genom.* **2013**, *12*, 58–65. [CrossRef]
16. Steri, M.; Idda, M.L.; Whalen, M.B.; Orrù, V. Genetic Variants in MRNA Untranslated Regions. *Wiley Interdiscip. Rev. RNA* **2018**, *9*, e1474. [CrossRef] [PubMed]
17. Patel, R.K.; West, J.D.; Jiang, Y.; Fogarty, E.A.; Grimson, A. Robust Partitioning of MicroRNA Targets from Downstream Regulatory Changes. *Nucleic Acids Res.* **2020**, *48*, 9724–9746. [CrossRef]
18. Kiltschewskij, D.J.; Harrison, P.F.; Fitzsimmons, C.; Beilharz, T.H.; Cairns, M.J. Extension of MRNA Poly(A) Tails and 3′UTRs during Neuronal Differentiation Exhibits Variable Association with Post-Transcriptional Dynamics. *Nucleic Acids Res.* **2023**, *51*, 8181–8198. [CrossRef]
19. Strober, B.J.; Elorbany, R.; Rhodes, K.; Krishnan, N.; Tayeb, K.; Battle, A.; Gilad, Y. Dynamic Genetic Regulation of Gene Expression during Cellular Differentiation HHS Public Access. *Science* **2019**, *364*, 1287–1290. [CrossRef]
20. Dinkova-Kostova, A.T.; Kostov, R.V.; Kazantsev, A.G. The Role of Nrf2 Signaling in Counteracting Neurodegenerative Diseases. *FEBS J.* **2018**, *285*, 3576–3590. [CrossRef]
21. Papp, D.; Lenti, K.; Módos, D.; Fazekas, D.; Dúl, Z.; Türei, D.; Földvári-Nagy, L.; Nussinov, R.; Csermely, P.; Korcsmáros, T. The NRF2-Related Interactome and Regulome Contain Multifunctional Proteins and Fine-Tuned Autoregulatory Loops. *FEBS Lett.* **2012**, *586*, 1795–1802. [CrossRef]
22. Nguyen, T.; Nioi, P.; Pickett, C.B. The Nrf2-Antioxidant Response Element Signaling Pathway and Its Activation by Oxidative Stress. *J. Biol. Chem.* **2009**, *284*, 13291–13295. [CrossRef] [PubMed]
23. Denicola, G.M.; Karreth, F.A.; Humpton, T.J.; Gopinathan, A.; Wei, C.; Frese, K.; Mangal, D.; Yu, K.H.; Yeo, C.J.; Calhoun, E.S.; et al. Oncogene-Induced Nrf2 Transcription Promotes ROS Detoxification and Tumorigenesis. *Nature* **2011**, *475*, 106–110. [CrossRef]
24. Bryan, H.K.; Olayanju, A.; Goldring, C.E.; Park, B.K. The Nrf2 Cell Defence Pathway: Keap1-Dependent and -Independent Mechanisms of Regulation. *Biochem. Pharmacol.* **2013**, *85*, 705–717. [CrossRef] [PubMed]
25. Jung, B.J.; Yoo, H.S.; Shin, S.; Park, Y.J.; Jeon, S.M. Dysregulation of NRF2 in Cancer: From Molecular Mechanisms to Therapeutic Opportunities. *Biomol. Ther.* **2018**, *26*, 57–68. [CrossRef] [PubMed]
26. Dhyani, N.; Tian, C.; Gao, L.; Rudebush, T.L.; Zucker, I.H. Nrf2-Keap1 in Cardiovascular Disease: Which Is the Cart and Which the Horse? *Physiology* **2024**, *39*, 288–301. [CrossRef]
27. Tucci, P.; Lattanzi, R.; Severini, C.; Saso, L. Nrf2 Pathway in Huntington's Disease (HD): What Is Its Role? *Int. J. Mol. Sci.* **2022**, *23*, 15272. [CrossRef]
28. Saha, S.; Buttari, B.; Profumo, E.; Tucci, P.; Saso, L. A Perspective on Nrf2 Signaling Pathway for Neuroinflammation: A Potential Therapeutic Target in Alzheimer's and Parkinson's Diseases. *Front. Cell. Neurosci.* **2022**, *15*, 787258. [CrossRef]
29. Wang, R.S.; Maron, B.A.; Loscalzo, J. Multiomics Network Medicine Approaches to Precision Medicine and Therapeutics in Cardiovascular Diseases. *Arterioscler. Thromb. Vasc. Biol.* **2023**, *43*, 493–503. [CrossRef]
30. Jurisic, V. Multiomic Analysis of Cytokines in Immuno-Oncology. *Expert Rev. Proteom.* **2020**, *17*, 663–674. [CrossRef]
31. Ngo, V.; Duennwald, M.L. Nrf2 and Oxidative Stress: A General Overview of Mechanisms and Implications in Human Disease. *Antioxidants* **2022**, *11*, 2345. [CrossRef]
32. Simmons, S.O.; Fan, C.-Y.; Yeoman, K.; Wakefield, J.; Ramabhadran, R. NRF2 Oxidative Stress Induced by Heavy Metals Is Cell Type Dependent. *Curr. Chem. Genom.* **2011**, *5*, 1–12. [CrossRef]
33. Kensler, T.W.; Wakabayashi, N.; Biswal, S. Cell Survival Responses to Environmental Stresses via the Keap1-Nrf2-ARE Pathway. *Annu. Rev. Pharmacol. Toxicol.* **2007**, *47*, 89–116. [CrossRef] [PubMed]

34. Heurtaux, T.; Bouvier, D.S.; Benani, A.; Helgueta Romero, S.; Frauenknecht, K.B.M.; Mittelbronn, M.; Sinkkonen, L. Normal and Pathological NRF2 Signalling in the Central Nervous System. *Antioxidants* **2022**, *11*, 1426. [CrossRef]
35. He, F.; Ru, X.; Wen, T. NRF2, a Transcription Factor for Stress Response and Beyond. *Int. J. Mol. Sci.* **2020**, *21*, 4777. [CrossRef]
36. Glanzner, W.G.; da Silva Sousa, L.R.; Gutierrez, K.; de Macedo, M.P.; Currin, L.; Perecin, F.; Bordignon, V. NRF2 Attenuation Aggravates Detrimental Consequences of Metabolic Stress on Cultured Porcine Parthenote Embryos. *Sci. Rep.* **2024**, *14*, 2973. [CrossRef]
37. Li, R.; Jia, Z.; Zhu, H. Regulation of Nrf2 Signaling. *React. Oxyg. Species (Apex)* **2019**, *8*, 312–322. [CrossRef] [PubMed]
38. Kumari, D.; Gabrielian, A.; Wheeler, D.; Usdin, K. The Roles of Sp1, Sp3, USF1/USF2 and NRF-1 in the Regulation and Three-Dimensional Structure of the Fragile X Mental Retardation Gene Promoter. *Biochem. J.* **2005**, *386*, 297–303. [CrossRef] [PubMed]
39. Takahashi, S.; Sugimoto, N. Watson-Crick versus Hoogsteen Base Pairs: Chemical Strategy to Encode and Express Genetic Information in Life. *Acc. Chem. Res.* **2021**, *54*, 2110–2120. [CrossRef]
40. Oumard, A.; Hennecke, M.; Hauser, H.; Nourbakhsh, M. Translation of NRF MRNA Is Mediated by Highly Efficient Internal Ribosome Entry. *Mol. Cell Biol.* **2000**, *20*, 2755–2759. [CrossRef]
41. Lee, D.S.M.; Ghanem, L.R.; Barash, Y. Integrative Analysis Reveals RNA G-Quadruplexes in UTRs Are Selectively Constrained and Enriched for Functional Associations. *Nat. Commun.* **2020**, *11*, 527. [CrossRef]
42. Otovat, F.; Bozorgmehr, M.R.; Mahmoudi, A.; Morsali, A. Porphyrin-Based Ligand Interaction with G-Quadruplex: Metal Cation Effects. *J. Mol. Recognit.* **2023**, *36*, e3017. [CrossRef] [PubMed]
43. Balaratnam, S.; Torrey, Z.R.; Calabrese, D.R.; Banco, M.T.; Yazdani, K.; Liang, X.; Fullenkamp, C.R.; Seshadri, S.; Holewinski, R.J.; Andresson, T.; et al. Investigating the NRAS 5′ UTR as a Target for Small Molecules. *Cell Chem. Biol.* **2023**, *30*, 643–657.e8. [CrossRef]
44. Lee, S.C.; Zhang, J.; Strom, J.; Yang, D.; Dinh, T.N.; Kappeler, K.; Chen, Q.M. G-Quadruplex in the NRF2 MRNA 5′ Untranslated Region Regulates De Novo NRF2 Protein Translation under Oxidative Stress. *Mol. Cell. Biol.* **2017**, *37*, e00122-16. [CrossRef] [PubMed]
45. Wu, S.; Jiang, L.; Lei, L.; Fu, C.; Huang, J.; Hu, Y.; Dong, Y.; Chen, J.; Zeng, Q. Crosstalk between G-Quadruplex and ROS. *Cell Death Dis.* **2023**, *14*, 37. [CrossRef]
46. Zang, H.; Mathew, R.O.; Cui, T. The Dark Side of Nrf2 in the Heart. *Front. Physiol.* **2020**, *11*, 722. [CrossRef]
47. Brüschweiler, S.; Fuchs, J.E.; Bader, G.; McConnell, D.B.; Konrat, R.; Mayer, M. A Step toward NRF2-DNA Interaction Inhibitors by Fragment-Based NMR Methods. *ChemMedChem* **2021**, *16*, 3576–3587. [CrossRef] [PubMed]
48. Poganik, J.R.; Long, M.J.C.; Disare, M.T.; Liu, X.; Chang, S.H.; Hla, T.; Aye, Y. Post-Transcriptional Regulation of Nrf2-MRNA by the MRNA-Binding Proteins HuR and AUF1. *FASEB J.* **2019**, *33*, 14636–14652. [CrossRef]
49. Kim, Y.S.; Kimball, S.R.; Piskounova, E.; Begley, T.J.; Hempel, N. Stress Response Regulation of MRNA Translation: Implications for Antioxidant Enzyme Expression in Cancer. *Proc. Natl. Acad. Sci. USA* **2024**, *121*, e2317846121. [CrossRef]
50. Akl, M.G.; Li, L.; Baccetto, R.; Phanse, S.; Zhang, Q.; Trites, M.J.; McDonald, S.; Aoki, H.; Babu, M.; Widenmaier, S.B. Complementary Gene Regulation by NRF1 and NRF2 Protects against Hepatic Cholesterol Overload. *Cell Rep.* **2023**, *42*, 112399. [CrossRef]
51. Tebay, L.E.; Robertson, H.; Durant, S.T.; Vitale, S.R.; Penning, T.M.; Dinkova-Kostova, A.T.; Hayes, J.D. Mechanisms of Activation of the Transcription Factor Nrf2 by Redox Stressors, Nutrient Cues, and Energy Status and the Pathways through Which It Attenuates Degenerative Disease. *Free Radic. Biol. Med.* **2015**, *88*, 108–146. [CrossRef] [PubMed]
52. Neupane, A.; Chariker, J.H.; Rouchka, E.C. Structural and Functional Classification of G-Quadruplex Families within the Human Genome. *Genes* **2023**, *14*, 645. [CrossRef]
53. Miskiewicz, J.; Sarzynska, J.; Szachniuk, M. How Bioinformatics Resources Work with G4 RNAs. *Brief. Bioinform.* **2021**, *22*, bbaa201.
54. Cagirici, H.B.; Budak, H.; Sen, T.Z. G4Boost: A Machine Learning-Based Tool for Quadruplex Identification and Stability Prediction. *BMC Bioinform.* **2022**, *23*, 240. [CrossRef]
55. Kikin, O.; D'Antonio, L.; Bagga, P.S. QGRS Mapper: A Web-Based Server for Predicting G-Quadruplexes in Nucleotide Sequences. *Nucleic Acids Res.* **2006**, *34*, W676–W682. [CrossRef]
56. Brázda, V.; Kolomazník, J.; Lýsek, J.; Bartas, M.; Fojta, M.; Šťastný, J.; Mergny, J.L. G4Hunter Web Application: A Web Server for G-Quadruplex Prediction. *Bioinformatics* **2019**, *35*, 3493–3495. [CrossRef]
57. Javadekar, S.M.; Nilavar, N.M.; Paranjape, A.; Das, K.; Raghavan, S.C. Characterization of G-Quadruplex Antibody Reveals Differential Specificity for G4 DNA Forms. *DNA Res.* **2020**, *27*, dsaa024. [CrossRef]
58. Lago, S.; Nadai, M.; Rossetto, M.; Richter, S.N. Surface Plasmon Resonance Kinetic Analysis of the Interaction between G-Quadruplex Nucleic Acids and an Anti-G-Quadruplex Monoclonal Antibody. *Biochim. Biophys. Acta Gen. Subj.* **2018**, *1862*, 1276–1282. [CrossRef] [PubMed]
59. Hellman, L.M.; Fried, M.G. Electrophoretic Mobility Shift Assay (EMSA) for Detecting Protein-Nucleic Acid Interactions. *Nat. Protoc.* **2007**, *2*, 1849–1861. [CrossRef] [PubMed]

60. Hou, Y.; Gan, T.; Fang, T.; Zhao, Y.; Luo, Q.; Liu, X.; Qi, L.; Zhang, Y.; Jia, F.; Han, J.; et al. G-Quadruplex Inducer/Stabilizer Pyridostatin Targets SUB1 to Promote Cytotoxicity of a Transplatinum Complex. *Nucleic Acids Res.* **2022**, *50*, 3070–3082. [CrossRef]
61. Rocca, R.; Talarico, C.; Moraca, F.; Costa, G.; Romeo, I.; Ortuso, F.; Alcaro, S.; Artese, A. Molecular Recognition of a Carboxy Pyridostatin toward G-Quadruplex Structures: Why Does It Prefer RNA? *Chem. Biol. Drug Des.* **2017**, *90*, 919–925. [CrossRef] [PubMed]
62. Liu, L.Y.; Ma, T.Z.; Zeng, Y.L.; Liu, W.; Mao, Z.W. Structural Basis of Pyridostatin and Its Derivatives Specifically Binding to G-Quadruplexes. *J. Am. Chem. Soc.* **2022**, *144*, 11878–11887. [CrossRef]
63. Zhang, X.; Spiegel, J.; Martínez Cuesta, S.; Adhikari, S.; Balasubramanian, S. Chemical Profiling of DNA G-Quadruplex-Interacting Proteins in Live Cells. *Nat. Chem.* **2021**, *13*, 626–633. [CrossRef]
64. Seo, M.; Lei, L.; Egli, M. Label-Free Electrophoretic Mobility Shift Assay (EMSA) for Measuring Dissociation Constants of Protein-RNA Complexes. *Curr. Protoc. Nucleic Acid. Chem.* **2019**, *76*, e70. [CrossRef]
65. Heffler, M.A.; Walters, R.D.; Kugel, J.F. Using Electrophoretic Mobility Shift Assays to Measure Equilibrium Dissociation Constants: GAL4-P53 Binding DNA as a Model System. *Biochem. Mol. Biol. Educ.* **2012**, *40*, 383–387. [CrossRef] [PubMed]
66. Sato, K.; Akiyama, M.; Sakakibara, Y. RNA Secondary Structure Prediction Using Deep Learning with Thermodynamic Integration. *Nat. Commun.* **2021**, *12*, 941. [CrossRef] [PubMed]
67. Horspool, D.R.; Coope, R.J.; Holt, R.A. Efficient Assembly of Very Short Oligonucleotides Using T4 DNA Ligase. *BMC Res. Notes* **2010**, *3*, 291. [CrossRef]
68. Fuller, C.W.; Richardson, C.C. Initiation of DNA Replication at the Primary Origin of Bacteriophage T7 by Purified Proteins. Initiation of bidirectional synthesis. *J. Biol. Chem.* **1985**, *260*, 3185–3196. [CrossRef]
69. Porecha, R.; Herschlag, D. RNA Radiolabeling. In *Methods in Enzymology*; Academic Press Inc.: Cambridge, MA, USA, 2013; Volume 530, pp. 255–279.
70. Yu, L.; Verwilst, P.; Shim, I.; Zhao, Y.Q.; Zhou, Y.; Kim, J.S. Fluorescent Visualization of Nucleolar G-Quadruplex Rna and Dynamics of Cytoplasm and Intranuclear Viscosity. *CCS Chem.* **2021**, *3*, 2725–2739. [CrossRef]
71. Dell'Oca, M.C.; Quadri, R.; Bernini, G.M.; Menin, L.; Grasso, L.; Rondelli, D.; Yazici, O.; Sertic, S.; Marini, F.; Pellicioli, A.; et al. Spotlight on G-Quadruplexes: From Structure and Modulation to Physiological and Pathological Roles. *Int. J. Mol. Sci.* **2024**, *25*, 3162. [CrossRef]
72. Hu, X.X.; Wang, S.Q.; Gan, S.Q.; Liu, L.; Zhong, M.Q.; Jia, M.H.; Jiang, F.; Xu, Y.; Xiao, C.D.; Shen, X.C. A Small Ligand That Selectively Binds to the G-Quadruplex at the Human Vascular Endothelial Growth Factor Internal Ribosomal Entry Site and Represses the Translation. *Front. Chem.* **2021**, *9*, 781198. [CrossRef]
73. Prestwood, P.R.; Yang, M.; Lewis, G.V.; Balaratnam, S.; Yazdani, K.; Schneekloth, J.S. Competitive Microarray Screening Reveals Functional Ligands for the DHX15 RNA G-Quadruplex. *ACS Med. Chem. Lett.* **2024**, *15*, 814–821. [CrossRef]
74. Mei, Y.; Deng, Z.; Vladimirova, O.; Gulve, N.; Johnson, F.B.; Drosopoulos, W.C.; Schildkraut, C.L.; Lieberman, P.M. TERRA G-Quadruplex RNA Interaction with TRF2 GAR Domain Is Required for Telomere Integrity. *Sci. Rep.* **2021**, *11*, 3509. [CrossRef]
75. Hashimoto, Y.; Kubo, H.; Kawauchi, K.; Miyoshi, D. NRAS DNA G-Quadruplex-Targeting Molecules for Sequence-Selective Enzyme Inhibition. *Chem. Commun.* **2024**, *60*, 13179–13182. [CrossRef] [PubMed]
76. Biffi, G.; Di Antonio, M.; Tannahill, D.; Balasubramanian, S. Visualization and Selective Chemical Targeting of RNA G-Quadruplex Structures in the Cytoplasm of Human Cells. *Nat. Chem.* **2014**, *6*, 75–80. [CrossRef] [PubMed]
77. Luo, L.; Jea, J.D.Y.; Wang, Y.; Chao, P.W.; Yen, L. Control of Mammalian Gene Expression by Modulation of PolyA Signal Cleavage at 5′ UTR. *Nat. Biotechnol.* **2024**, *42*, 1454–1466. [CrossRef]
78. Van Drie, J.H.; Tong, L. Cryo-EM as a Powerful Tool for Drug Discovery. *Bioorg. Med. Chem. Lett.* **2020**, *30*, 127524. [CrossRef]
79. Wu, G.; Tillo, D.; Ray, S.; Chang, T.C.; Schneekloth, J.S.; Vinson, C.; Yang, D. Custom G4 Microarrays Reveal Selective G-Quadruplex Recognition of Small Molecule BMVC: A Large-Scale Assessment of Ligand Binding Selectivity. *Molecules* **2020**, *25*, 3465. [CrossRef]
80. Castillo-González, D.; Pérez-Machado, G.; Pallardó, F.; Garrigues-Pelufo, T.-M.; Cabrera-Pérez, M.-A. Computational Tools in the Discovery of New G-Quadruplex Ligands with Potential Anticancer Activity. *Curr. Top. Med. Chem.* **2012**, *12*, 2843–2856. [CrossRef] [PubMed]
81. McPherson, A.; Cudney, B. Optimization of Crystallization Conditions for Biological Macromolecules. *Acta Crystallogr. F Struct. Biol. Commun.* **2014**, *70*, 1445–1467. [CrossRef]
82. Marion, D. An Introduction to Biological NMR Spectroscopy. *Mol. Cell. Proteom.* **2013**, *12*, 3006–3025. [CrossRef]
83. Yadav, D.K.; Lukavsky, P.J. NMR Solution Structure Determination of Large RNA-Protein Complexes. *Prog. Nucl. Magn. Reson. Spectrosc.* **2016**, *97*, 57–81. [CrossRef] [PubMed]
84. Maleki, P.; Budhathoki, J.B.; Roy, W.A.; Balci, H. A Practical Guide to Studying G-Quadruplex Structures Using Single-Molecule FRET. *Mol. Genet. Genom.* **2017**, *292*, 483–498. [CrossRef] [PubMed]
85. Masson, T.; Guetta, C.L.; Laigre, E.; Cucchiarini, A.; Duchambon, P.; Teulade-Fichou, M.P.; Verga, D. BrdU Immuno-Tagged G-Quadruplex Ligands: A New Ligand-Guided Immunofluorescence Approach for Tracking G-Quadruplexes in Cells. *Nucleic Acids Res.* **2021**, *49*, 12644–12660. [CrossRef]

86. Kusi-Appauh, N.; Ralph, S.F.; van Oijen, A.M.; Spenkelink, L.M. Understanding G-Quadruplex Biology and Stability Using Single-Molecule Techniques. *J. Phys. Chem. B* **2023**, *127*, 5521–5540. [CrossRef]
87. Meiser, N.; Fuks, C.; Hengesbach, M. Cooperative Analysis of Structural Dynamics in RNA-Protein Complexes by Single-Molecule Förster Resonance Energy Transfer Spectroscopy. *Molecules* **2020**, *25*, 2057. [CrossRef]
88. Geraets, J.A.; Pothula, K.R.; Schröder, G.F. Integrating Cryo-EM and NMR Data. *Curr. Opin. Struct. Biol.* **2020**, *61*, 173–181. [CrossRef]
89. Rouleau, S.G.; Garant, J.M.; Bolduc, F.; Bisaillon, M.; Perreault, J.P. G-Quadruplexes Influence Pri-MicroRNA Processing. *RNA Biol.* **2018**, *15*, 198–206. [CrossRef] [PubMed]
90. Jayaraj, G.G.; Pandey, S.; Scaria, V.; Maiti, S. Potential G-Quadruplexes in the Human Long Non-Coding Transcriptome. *RNA Biol.* **2012**, *9*, 81–89. [CrossRef]
91. Dumas, L.; Herviou, P.; Dassi, E.; Cammas, A.; Millevoi, S. G-Quadruplexes in RNA Biology: Recent Advances and Future Directions. *Trends Biochem. Sci.* **2021**, *46*, 270–283. [CrossRef]
92. Shu, H.; Zhang, R.; Xiao, K.; Yang, J.; Sun, X. G-Quadruplex-Binding Proteins: Promising Targets for Drug Design. *Biomolecules* **2022**, *12*, 648. [CrossRef]
93. Cammas, A.; Desprairies, A.; Dassi, E.; Millevoi, S. The Shaping of MRNA Translation Plasticity by RNA G-Quadruplexes in Cancer Progression and Therapy Resistance. *NAR Cancer* **2024**, *6*, zcae025. [CrossRef]
94. Herdy, B.; Mayer, C.; Varshney, D.; Marsico, G.; Murat, P.; Taylor, C.; D'Santos, C.; Tannahill, D.; Balasubramanian, S. Analysis of NRAS RNA G-Quadruplex Binding Proteins Reveals DDX3X as a Novel Interactor of Cellular G-Quadruplex Containing Transcripts. *Nucleic Acids Res.* **2018**, *46*, 11592–11604. [CrossRef]
95. Weng, H.Y.; Huang, H.L.; Zhao, P.P.; Zhou, H.; Qu, L.H. Translational Repression of Cyclin D3 by a Stable G-Quadruplex in Its 5′ UTR: Implications for Cell Cycle Regulation. *RNA Biol.* **2012**, *9*, 1099–1109. [CrossRef]
96. Kharel, P.; Ivanov, P. RNA G-Quadruplexes and Stress: Emerging Mechanisms and Functions. *Trends Cell Biol.* **2024**, *34*, 771–784. [CrossRef]
97. Kumari, S.; Bugaut, A.; Huppert, J.L.; Balasubramanian, S. An RNA G-Quadruplex in the 5′ UTR of the NRAS Proto-Oncogene Modulates Translation. *Nat. Chem. Biol.* **2007**, *3*, 218–221. [CrossRef]
98. Morris, M.J.; Basu, S. An Unusually Stable G-Quadruplex within the 5′-UTR of the MT3 Matrix Metalloproteinase MRNA Represses Translation in Eukaryotic Cells. *Biochemistry* **2009**, *48*, 5313–5319. [CrossRef]
99. Morris, M.J.; Negishi, Y.; Pazsint, C.; Schonhoft, J.D.; Basu, S. An RNA G-Quadruplex Is Essential for Cap-Independent Translation Initiation in Human VEGF IRES. *J. Am. Chem. Soc.* **2010**, *132*, 17831–17839. [CrossRef] [PubMed]
100. Koukouraki, P.; Doxakis, E. Constitutive Translation of Human A-Synuclein Is Mediated by the 50-Untranslated Region. *Open Biol.* **2016**, *6*, 160022. [CrossRef] [PubMed]
101. Thakur, R.K.; Kumar, P.; Halder, K.; Verma, A.; Kar, A.; Parent, J.L.; Basundra, R.; Kumar, A.; Chowdhury, S. Metastases Suppressor NM23-H2 Interaction with G-Quadruplex DNA within c-MYC Promoter Nuclease Hypersensitive Element Induces c-MYC Expression. *Nucleic Acids Res.* **2009**, *37*, 172–183. [CrossRef] [PubMed]
102. Kamzeeva, P.N.; Alferova, V.A.; Korshun, V.A.; Varizhuk, A.M.; Aralov, A. V 5′-UTR G-Quadruplex-Mediated Translation Regulation in Eukaryotes: Current Understanding and Methodological Challenges. *Int. J. Mol. Sci.* **2025**, *26*, 1187. [CrossRef]
103. Qi, Q.; Liu, X.; Xiong, W.; Zhang, K.; Shen, W.; Zhang, Y.; Xu, X.; Zhong, C.; Zhang, Y.; Tian, T.; et al. Reducing CRISPR-Cas9 off-Target Effects by Optically Controlled Chemical Modifications of Guide RNA. *Cell Chem. Biol.* **2024**, *31*, 1839–1851. [CrossRef]
104. Yoneyama, M.; Kikuchi, M.; Natsukawa, T.; Shinobu, N.; Imaizumi, T.; Miyagishi, M.; Taira, K.; Akira, S.; Fujita, T. The RNA Helicase RIG-I Has an Essential Function in Double-Stranded RNA-Induced Innate Antiviral Responses. *Nat. Immunol.* **2004**, *5*, 730–737. [CrossRef] [PubMed]
105. Stevens, A.J.; de Jong, L.; Kennedy, M.A. The Dynamic Regulation of G-Quadruplex DNA Structures by Cytosine Methylation. *Int. J. Mol. Sci.* **2022**, *23*, 2407. [CrossRef]
106. Vorlíčková, M.; Kejnovská, I.; Sagi, J.; Renčiuk, D.; Bednářová, K.; Motlová, J.; Kypr, J. Circular Dichroism and Guanine Quadruplexes. *Methods* **2012**, *57*, 64–75. [CrossRef] [PubMed]
107. Zou, M.; Li, J.Y.; Zhang, M.J.; Li, J.H.; Huang, J.T.; You, P.D.; Liu, S.W.; Zhou, C.Q. G-Quadruplex Binder Pyridostatin as an Effective Multi-Target ZIKV Inhibitor. *Int. J. Biol. Macromol.* **2021**, *190*, 178–188. [CrossRef]
108. Rodriguez, R.; Miller, K.M.; Forment, J.V.; Bradshaw, C.R.; Nikan, M.; Britton, S.; Oelschlaegel, T.; Xhemalce, B.; Balasubramanian, S.; Jackson, S.P. Small-Molecule-Induced DNA Damage Identifies Alternative DNA Structures in Human Genes. *Nat. Chem. Biol.* **2012**, *8*, 301–310. [CrossRef] [PubMed]
109. Roy, S.; Ali, A.; Bhattacharya, S. Theoretical Insight into the Library Screening Approach for Binding of Intermolecular G-Quadruplex RNA and Small Molecules through Docking and Molecular Dynamics Simulation Studies. *J. Phys. Chem. B* **2021**, *125*, 5489–5501. [CrossRef]
110. Dickerhoff, J.; Warnecke, K.R.; Wang, K.; Deng, N.; Yang, D. Evaluating Molecular Docking Software for Small Molecule Binding to G-Quadruplex DNA. *Int. J. Mol. Sci.* **2021**, *22*, 10801. [CrossRef]

111. Peng, R.; Huang, Q.; Wang, L.; Qiao, G.; Huang, X.; Jiang, J.; Chu, X. G-quadruplex RNA Based PROTAC Enables Targeted Degradation of RNA Binding Protein FMRP for Tumor Immunotherapy. *Angew. Chem. Int. Ed.* **2024**, *136*, e202402715. [CrossRef]
112. Zhai, L.Y.; Liu, J.F.; Zhao, J.J.; Su, A.M.; Xi, X.G.; Hou, X.M. Targeting the RNA G-Quadruplex and Protein Interactome for Antiviral Therapy. *J. Med. Chem.* **2022**, *65*, 10161–10182. [CrossRef] [PubMed]
113. Virgilio, A.; Amato, T.; Petraccone, L.; Esposito, F.; Grandi, N.; Tramontano, E.; Romero, R.; Haider, S.; Gomez-Monterrey, I.; Novellino, E.; et al. Improvement of the Activity of the Anti-HIV-1 Integrase Aptamer T30175 by Introducing a Modified Thymidine into the Loops. *Sci. Rep.* **2018**, *8*, 7447. [CrossRef] [PubMed]
114. Esposito, V.; Pirone, L.; Mayol, L.; Pedone, E.; Virgilio, A.; Galeone, A. Exploring the Binding of d(GGGT)4 to the HIV-1 Integrase: An Approach to Investigate G-Quadruplex Aptamer/Target Protein Interactions. *Biochimie* **2016**, *127*, 19–22. [CrossRef] [PubMed]

Disclaimer/Publisher's Note: The statements, opinions and data contained in all publications are solely those of the individual author(s) and contributor(s) and not of MDPI and/or the editor(s). MDPI and/or the editor(s) disclaim responsibility for any injury to people or property resulting from any ideas, methods, instructions or products referred to in the content.